Supporting Information

Customization Nanoscale Interfacial Solvation Structure for Low Temperature Lithium Metal Batteries

Nan Li,[‡a] Kun Gao,[‡c] Ke Fan,[‡a] Li Ma,[c] Zihao Li,[c] Baoluo He,[c] Chao Shen,[c] Qian Ye, *[c] Keyu Xie,*[bc] and Haitao Huang*[a]

[a] Department of Applied Physics and Research Institute for Smart Energy, The Hong Kong Polytechnic University, Hong Kong, P.R. China.

[b] Institute of Clean Energy, Yangtze River Delta Research Institute, Northwestern Polytechnical University, Taicang 215400, China.

[c] State Key Laboratory of Solidification Processing, Center for Nano Energy Materials, School of Materials Science and Engineering, Northwestern Polytechnical University and Shaanxi Joint Laboratory of Graphene (NPU), Xi'an 710072, P.R. China.

[‡] These authors contributed equally: Nan Li, Kun Gao, Ke Fan.

*e-mail: yeqian213@nwpu.edu.cn (Q. Ye); kyxie@nwpu.edu.cn (K. Y. Xie); aphhuang@polyu.edu.hk (H. T. Huang)

Supplementary Figures

In following content, the E1 and E2 refers to 1M LiTFSI in DOL/DME (1:1 in volume) and 1M $LiPF_6$ in EC/DEC/EMC (1:1:1 in volume), respectively.
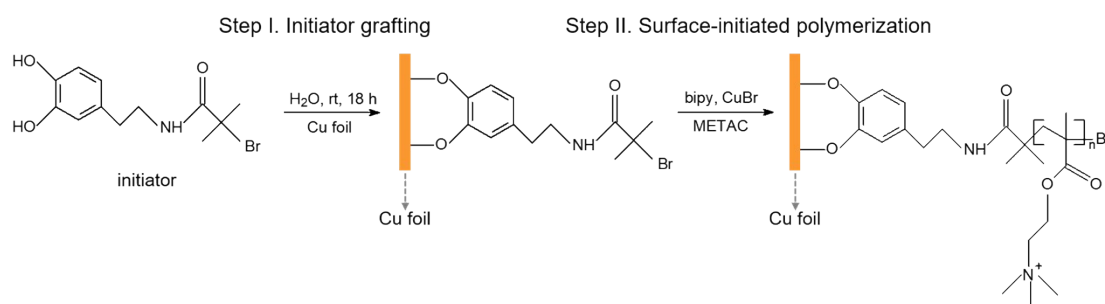
Fig. S1 Preparation of PMETAC polymer brushes grafted Cu substrates.
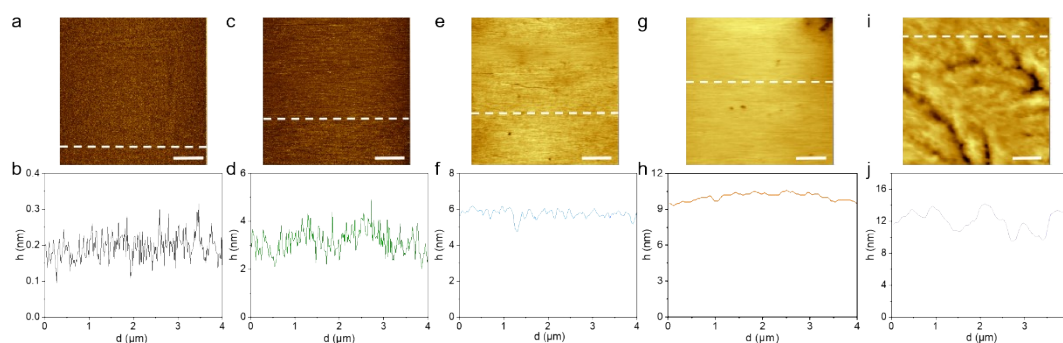
Fig. S2 AFM images of PMETAC polymer brushes with various polymerization time of (a) 0 min, (c) 15 min, (e) 30 min, (g) 60 min, and (i) 75 min, and the corresponding thickness analysis of (b) bare mica, (d) P_{15}@mica, (f) P_{30}@mica, (h) P_{60}@mica, and (j) P_{75}@mica, respectively. Mica was selected as the substrate to evaluate the polymer thickness due to its atomically flat surface. The scale bars in a, c, e, g, and i are 1 μm.
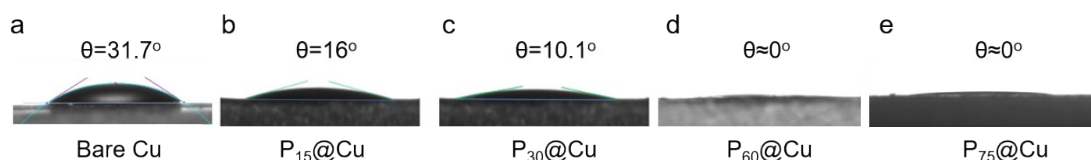
Fig. S3 Contact angles of the electrolyte on (a) bare Cu, (b) P_{15}@Cu, (c) P_{30}@Cu, (d) P_{60}@Cu,and (e) P_{75}@Cu substrates, respectively.
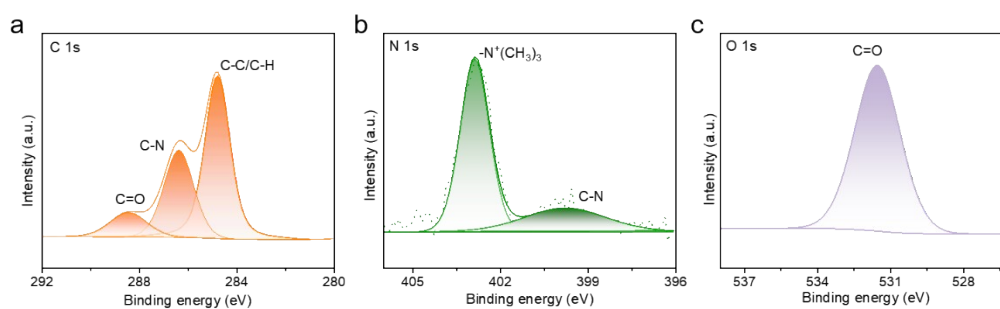
Fig. S4 (a) C 1s, (b) N 1s, and (c) O 1s core-level XPS spectra of PMETAC polymer brushes.
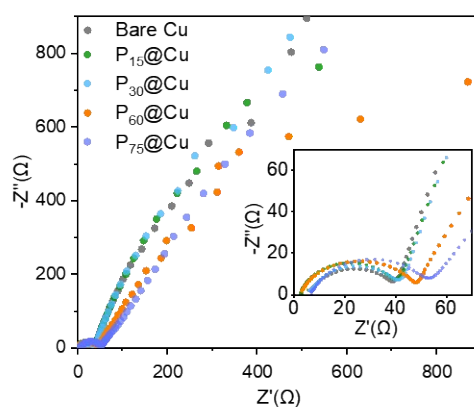
Fig. S5 The EIS of bare Cu foil, P_{15}@Cu, P_{30}@Cu, P_{60}@Cu, and P_{75}@Cu substrates, respectively.

The charge-transfer resistance of bare Cu foil, P_{15}@Cu, P_{30}@Cu, P_{60}@Cu, and P_{75}@Cu substrates are 37.82, 39.52, 39.79, 47.21, and 50.19 ohm, respectively. As can

be seen, the impedance parameters of $P_{15}@Cu$, $P_{30}@Cu$, $P_{60}@Cu$ substrates display

slight increase compared with bare Cu foil, while the resistance of $P_{75}@Cu$ substrate is

significantly larger than that of bare Cu foil, which may be attributed to the thicker

polymer brush layer grafted on the surface of Cu.
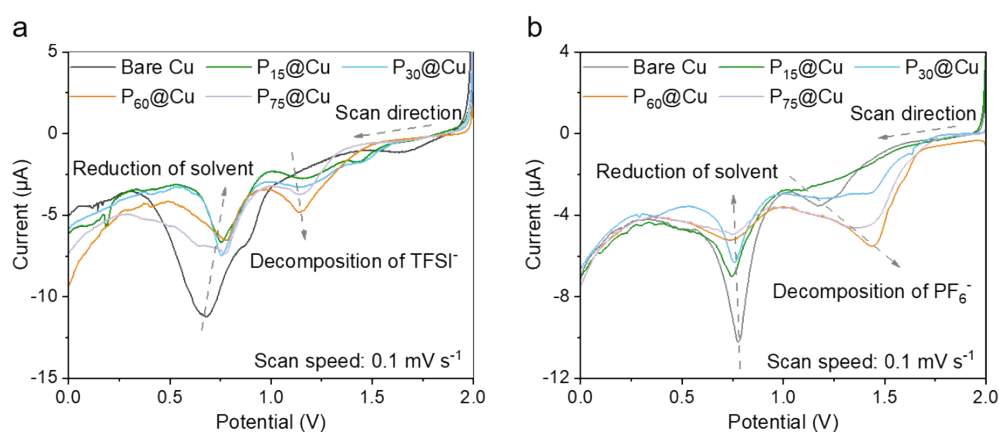
Fig. S6 Typical CV curves of Li-Cu cells with different Cu substrates.
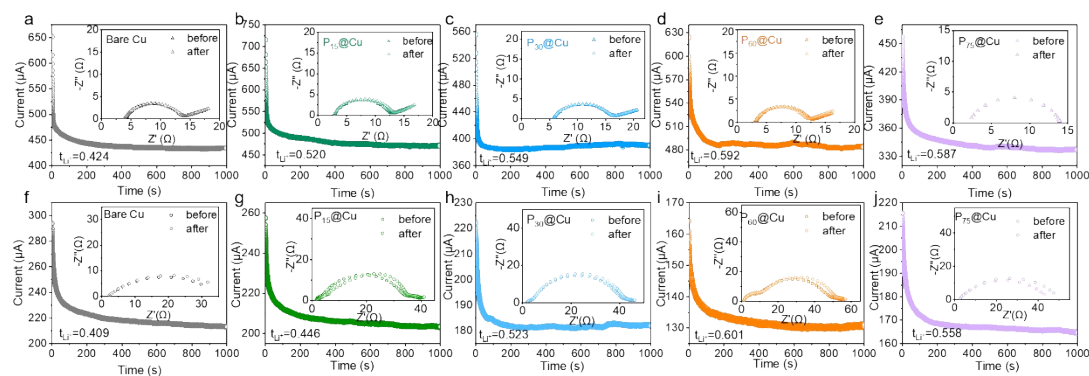
Fig. S7 The EIS and characteristic Li^+ transference number of symmetrical cells in E1

with (a) bare Cu foil, (b) $P_{15}@Cu$, (c) $P_{30}@Cu$, (d) $P_{60}@Cu$, and (e) $P_{75}@Cu$ substrates.

The EIS and characteristic Li^+ transference number of symmetrical cells in E2 with (f)

bare Cu foil, (g) $P_{15}@Cu$, (h) $P_{30}@Cu$, (i) $P_{60}@Cu$, and (j) $P_{75}@Cu$ substrates.
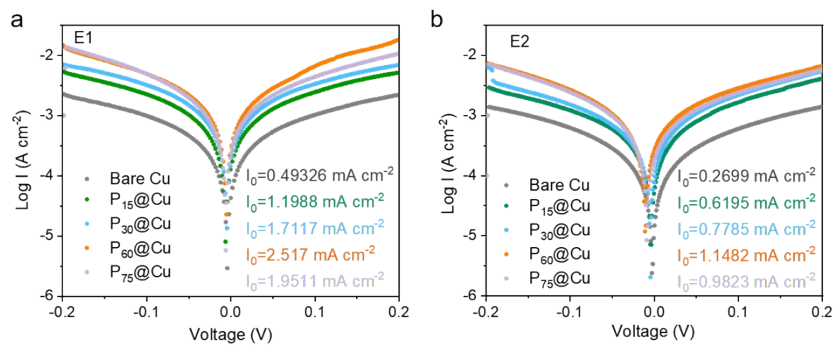
Fig. S8 The Tafel slopes and corresponding exchange current densities of various substrates in (a) E1 and (b) E2.
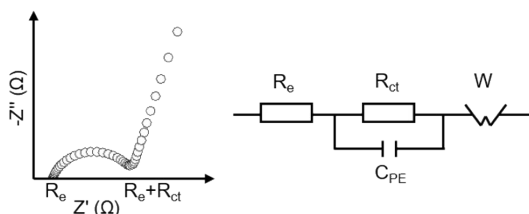
Fig. S9 The schematic Nyquist plot and the equivalent circuit model for EIS spectra.
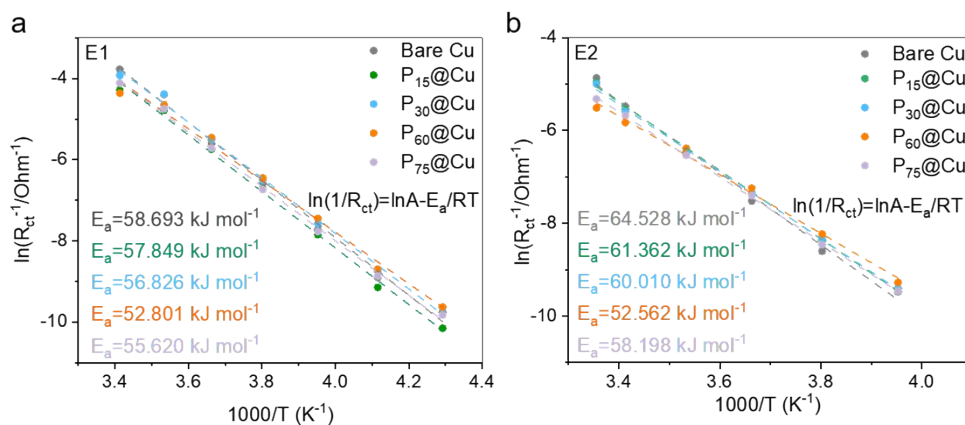
Fig. S10 Arrhenius behavior and corresponding activation energies of various substrates in (a) E1 and (b) E2.
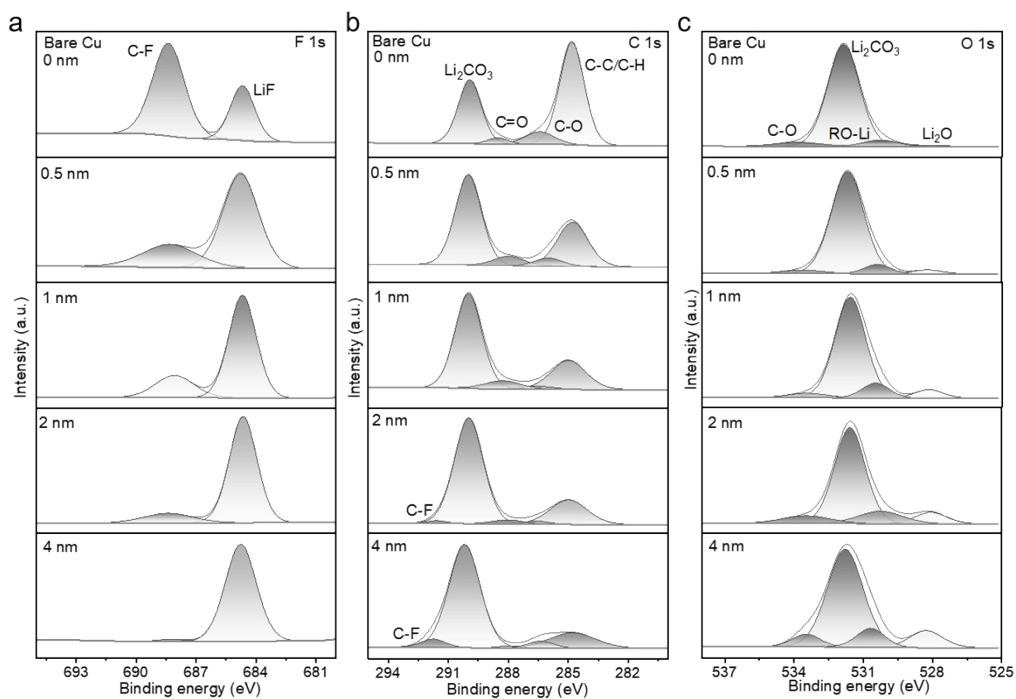
Fig. S11 (a) F 1s, (b) C 1s, and (c) O 1s core-level XPS spectra of SEI formed on bare Cu foil in E1 electrolyte at different etching depths of 0, 0.5, 1, 2, 4 nm.

The typical peaks of SEI components, C-F (688.37 eV) and LiF (684.67 eV) in F 1S core-level, and C-F (291.77 eV), Li_2CO_3 (289.9 eV), C=O (288.5 eV), C-O (286.4 eV) and C-C/C-H (284.8 eV) in C 1S core-level, as well as RO-Li (530.87 eV) and Li_2O (528.27 eV) in O 1S core-level, can be observed.[1]
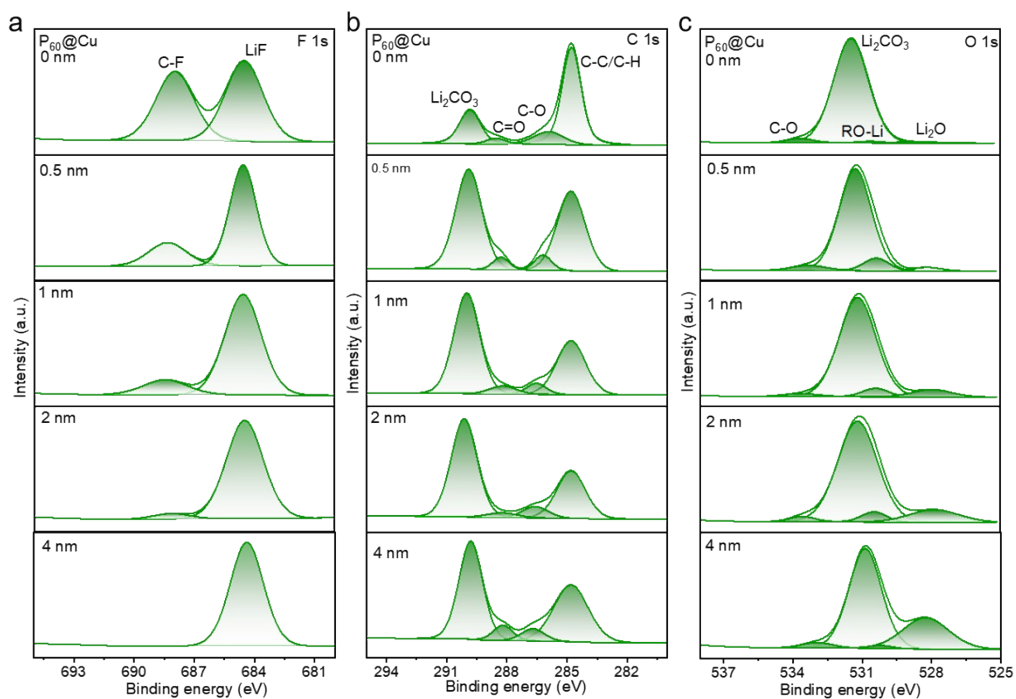
Fig. S12 (a) F 1s, (b) C 1s, and (c) O 1s core-level XPS spectra of SEI formed on

PMETAC grafted Cu substrate in E1 electrolyte at different etching depths of 0, 0.5, 1,
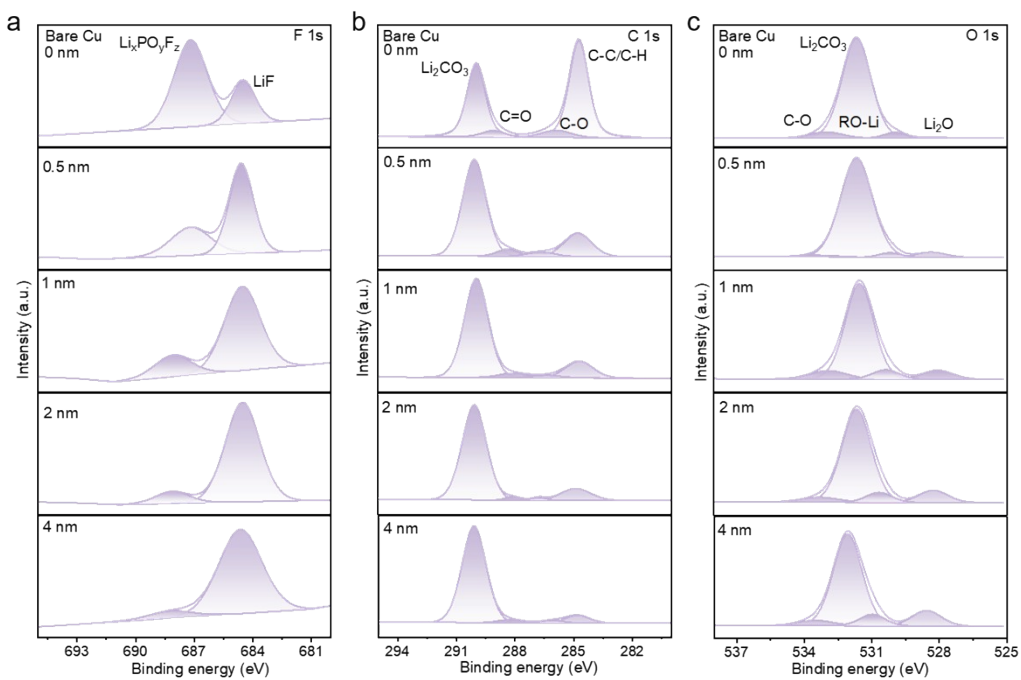
2, 4 nm.

Fig. S13 (a) F 1s, (b) C 1s, and (c) O 1s core-level XPS spectra of SEI formed on bare

Cu foil in E2 electrolyte at different etching depths of 0, 0.5, 1, 2, 4 nm.

The typical peaks of SEI components, $Li_xPO_yF_z$ (687.97 eV) and LiF (684.67 eV) in F 1S core-level, and Li_2CO_3 (289.9 eV), C=O (288.5 eV), C-O (286.4 eV) and C-C/C-H (284.8 eV) in C 1S core-level, as well as RO-Li (530.87 eV) and Li_2O (528.27 eV) in O 1S core-level, can be observed.[2]
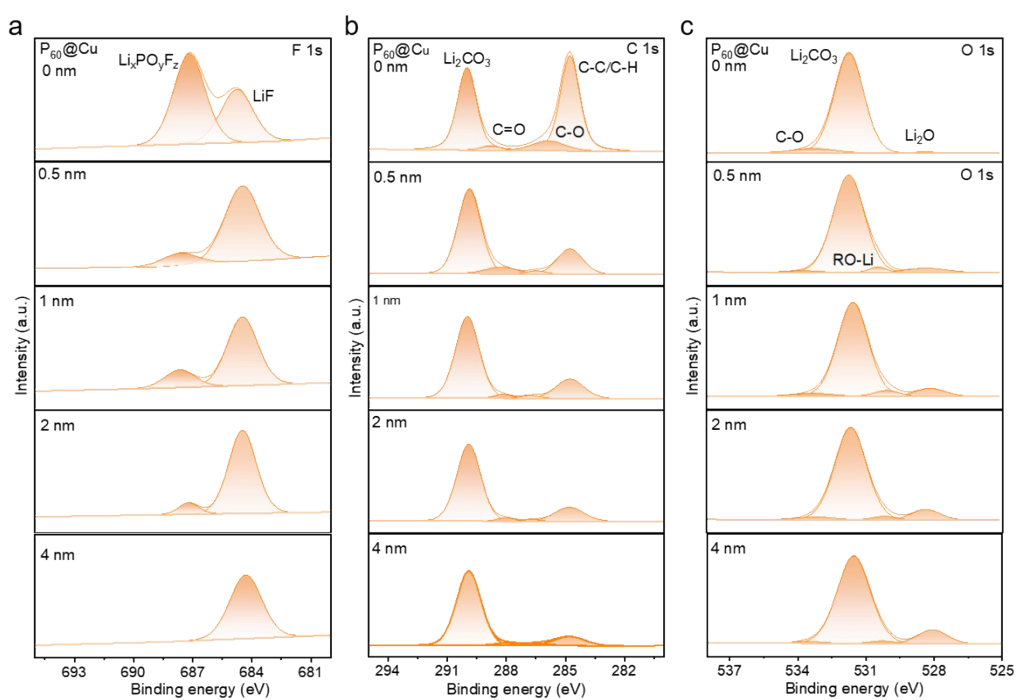
Fig. S14 (a) F 1s, (b) C 1s, and (c) O 1s core-level XPS spectra of SEI formed on PMETAC grafted Cu substrate in E2 electrolyte at different etching depths of 0, 0.5, 1, 2, 4 nm.
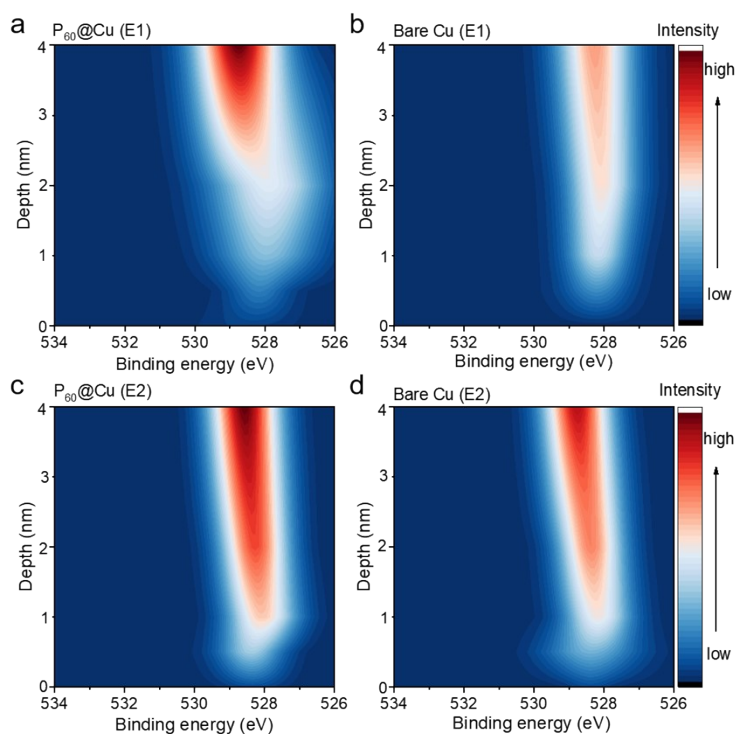
Fig. S15 (a, b) Change of Li_2O content with etching depth on PMETAC grafted Cu substrate and bare Cu foil in E1 electrolyte. (c, d) Change of Li_2O content with etching depth on PMETAC grafted Cu substrate and bare Cu foil in E2 electrolyte.

The content of Li_2O in SEI of PMETAC grafted Cu substrates displays obvious enhancement compared with its counterpart in both ether-based and ester-based electrolytes.
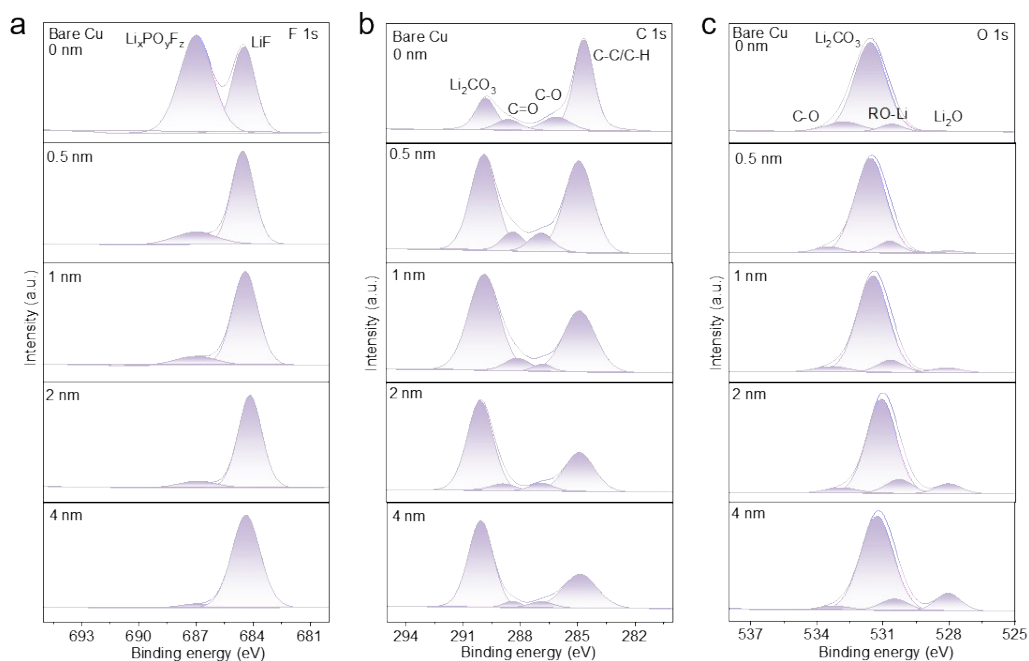
Fig. S16 (a) F 1s, (b) C 1s, and (c) O 1s core-level XPS spectra of SEI with 3 mAh cm^{-2}

Li metal deposit on bare Cu foil at different etching depths of 0, 0.5, 1, 2, 4 nm.
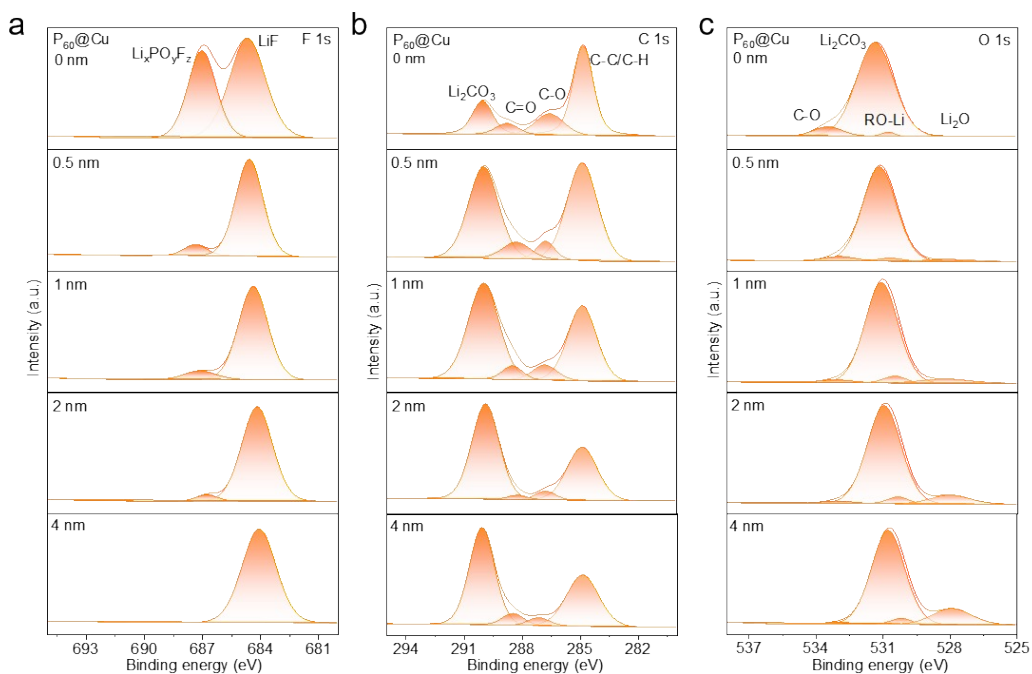
Fig. S17 (a) F 1s, (b) C 1s, and (c) O 1s core-level XPS spectra of SEI with 3 mAh cm^{-2}

Li metal deposit on PMETAC grafted Cu substrate at different etching depths of 0, 0.5,

1, 2, 4 nm.
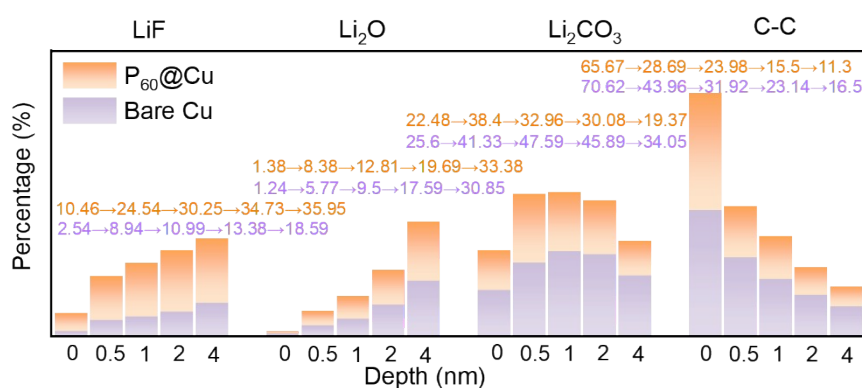
Fig. S18 Comparison of key components of SEI with 3 mAh cm^{-2} Li metal deposit on various substrates.

After electrodepositing 3 mAh cm^{-2} Li metal on bare Cu foil and PMETAC grafted Cu substrate, the depth profile of key SEI components were analyze. As can be seen, with the increase of etching depth, the inorganic contents of LiF and Li$_2$O increase gradually, while the contents of C-C and Li$_2$CO$_3$ decrease obviously, which demonstrate similar structure and composition to the SEI formed at initial electrodeposition, indicating that the induced inorganic-rich SEI is stable and further confirming the regulation of PMETAC polymer brushes on nanoscale interfacial solvation structure.
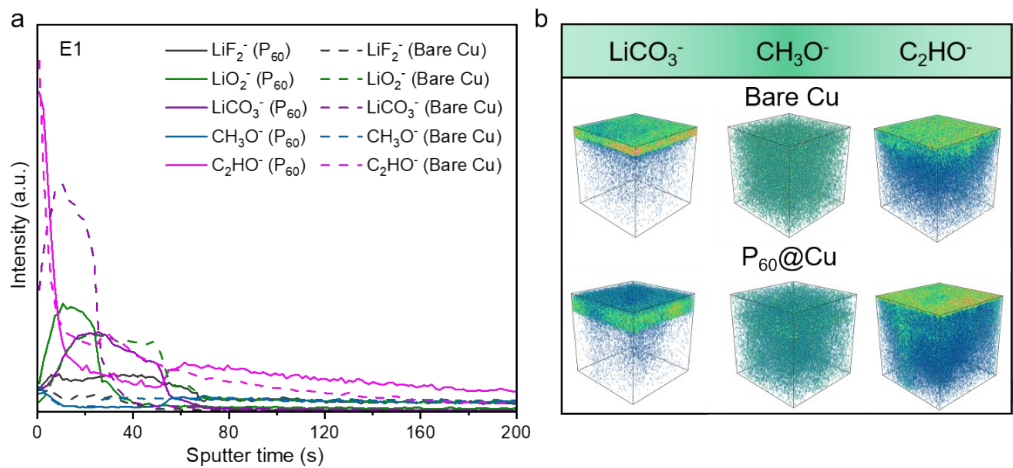
Fig. S19 (a) Normalized TOF-SIMS depth profiles of various secondary ion fragments in SEI on different substrates formed in E1 electrolyte. (b) TOF-SIMS 3D distribution of secondary ion fragments in SEI on different substrates formed in E1 electrolyte. The upper row is bare Cu foil and the lower row is PMETAC grafted Cu substrate.
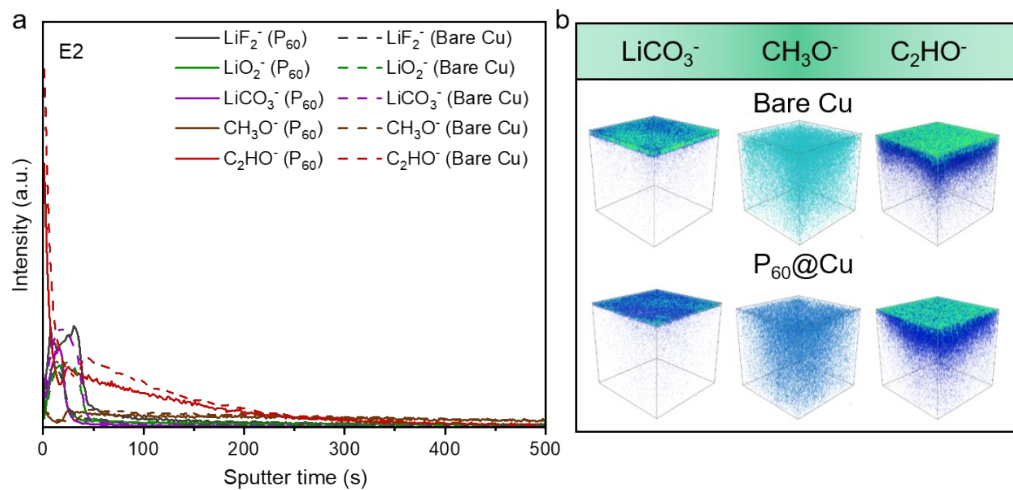
Fig. S20 (a) Normalized TOF-SIMS depth profiles of various secondary ion fragments in SEI on different substrates formed in E2 electrolyte. (b) TOF-SIMS 3D distribution of secondary ion fragments in SEI on different substrates formed in E2 electrolyte. The upper row is bare Cu foil and the lower row is PMETAC grafted Cu substrate.
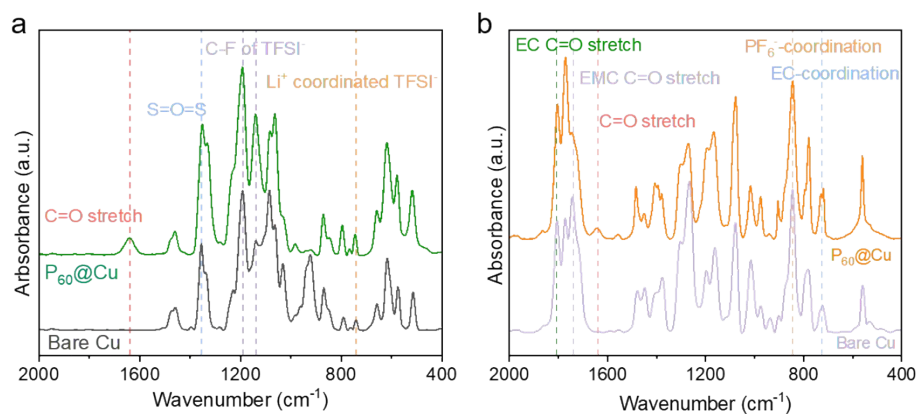
Fig. S21 (a) ATR spectra of interfacial solvation structures on bare Cu foil and PMETAC grafted Cu substrate in E1 electrolyte. (b) ATR spectra of interfacial solvation structures on bare Cu foil and PMETAC grafted Cu substrate in E2 electrolyte.

The peak around 744 cm^{-1} and 843 cm^{-1} reflect the coordination structure of Li$^+$ with TFSI$^-$, and the coordination structure of Li$^+$ with PF$_6^-$, respectively.[3]
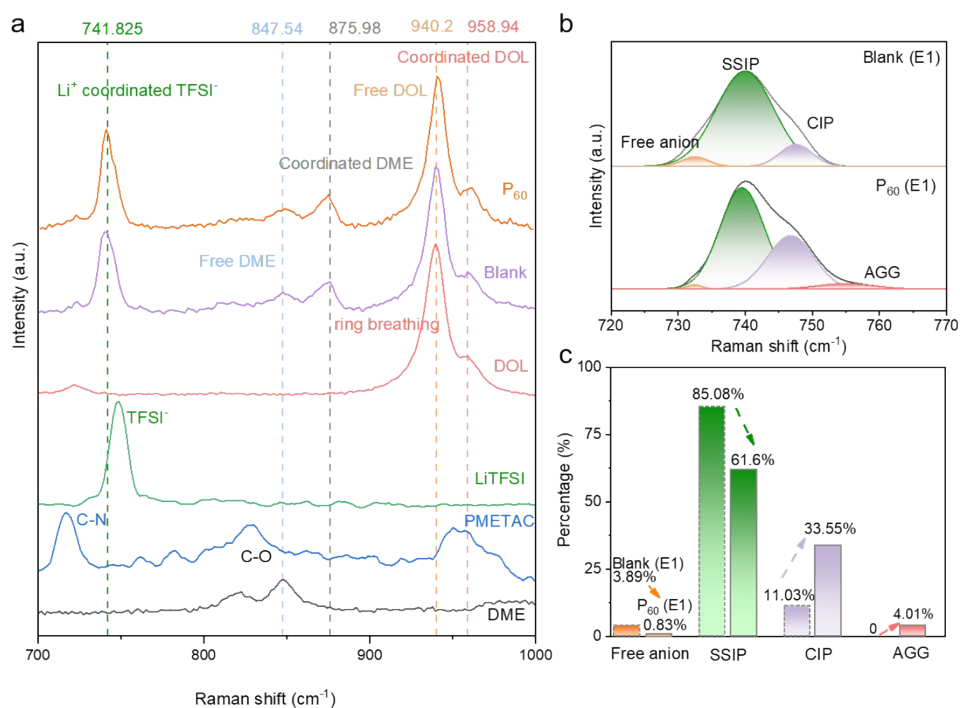
Fig. S22 (a) Raman spectra of E1 electrolyte with PMETAC. (b) Raman spectra of various solvation structures under E1 electrolyte with PMETAC. (c) The percentage of different solvation structures. The dashed frame represents blank E1 (i.e., without PMETAC), and the solid one represents E1 with PMETAC.

The peak around 742 cm^{-1} represents the coordination of Li$^+$ with TFSI$^-$.[4] With the cooperation of PMETAC, this peak displays significant enhancement with slight broadening towards upfield. The detailed solvation structure can be achieved with further peak deconvolution (Fig.S22b). As can be seen, the percentage of SSIP is obviously decreased, while the percentages of CIP and AGG are increased by over 3 times (Fig. S22c).
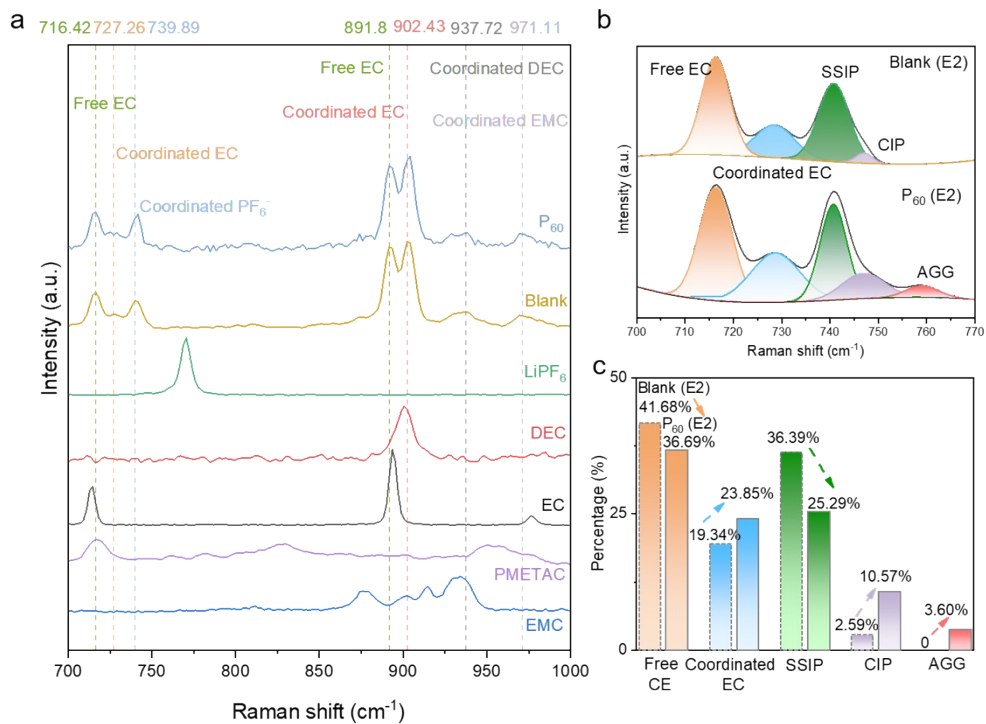
Fig. S23 (a) Raman spectra of E2 electrolyte with PMETAC. (b) Raman spectra of various solvation structures under E2 electrolyte with PMETAC. (c) The percentage of different solvation structures. The dashed frame represents blank E2 (i.e., without PMETAC), and the solid one represents E2 with PMETAC.

The peak around 740 cm^{-1} represent the coordination of Li$^+$ with PF$_6^-$.[5] With the cooperation of PMETAC, this peak displays enhancement and a slight upfield displacement. The detailed solvation structure can be achieved with further peak deconvolution (Fig. S23b). Similar transformation trend of solvation structure can be also observed in E2 electrolyte. As can be seen, the percentage of SSIP is significantly decreased, while the percentages of CIP and AGG are obviously increased to 10.57% and 3.60%, respectively (Fig. S23c).
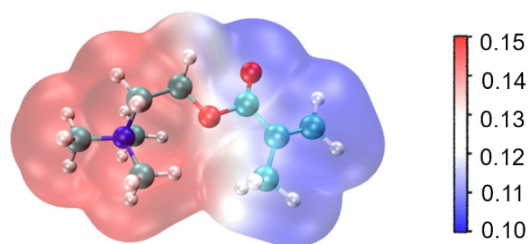
Fig. S24 The electrostatic potential map of monomer. The red, blue, cyan and white balls represent O, N, C, H, respectively.
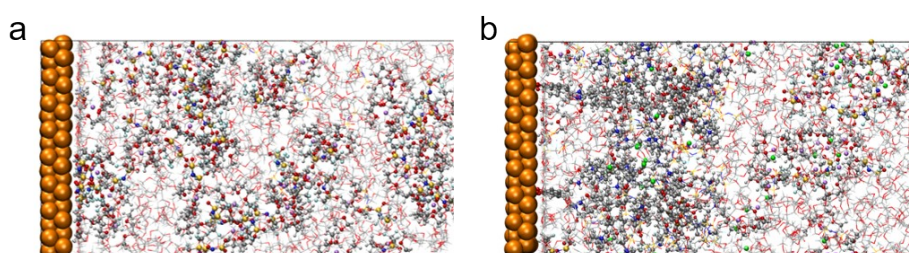
Fig. S25 The established simulation models on (a) bare Cu foil and (b) PMETAC grafted Cu substrate.
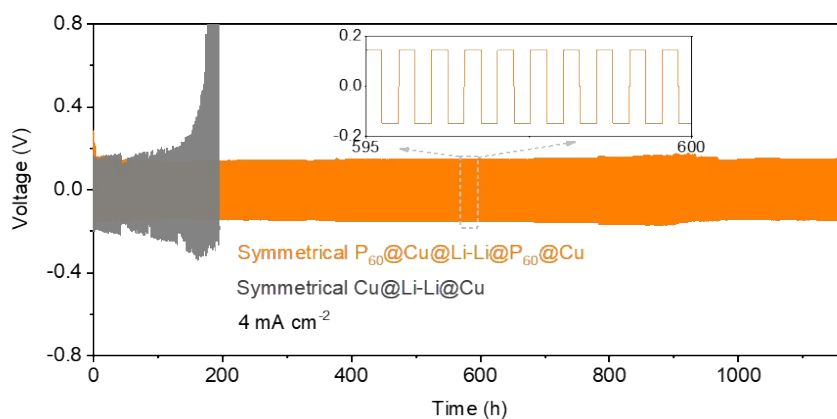
Fig. S26 Voltage-time curves of Li deposition/stripping in the symmetrical cells. The inset shows detailed voltage profiles of 595 to 600 h. The current density is 4.0 mA cm^{-2}.
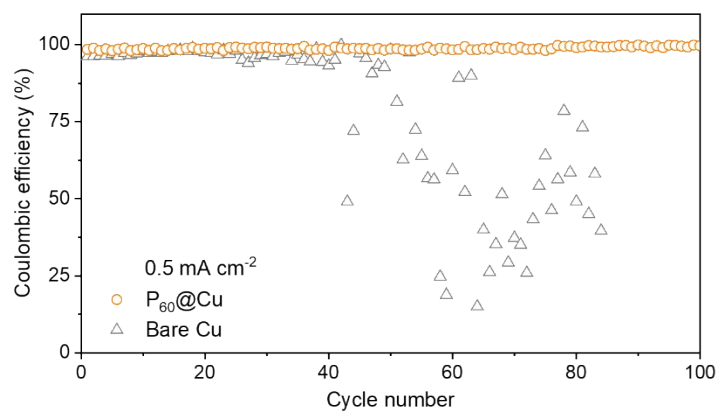
Fig. S27 CEs of different anodes at current densities of 0.5 mA cm^{-2}.
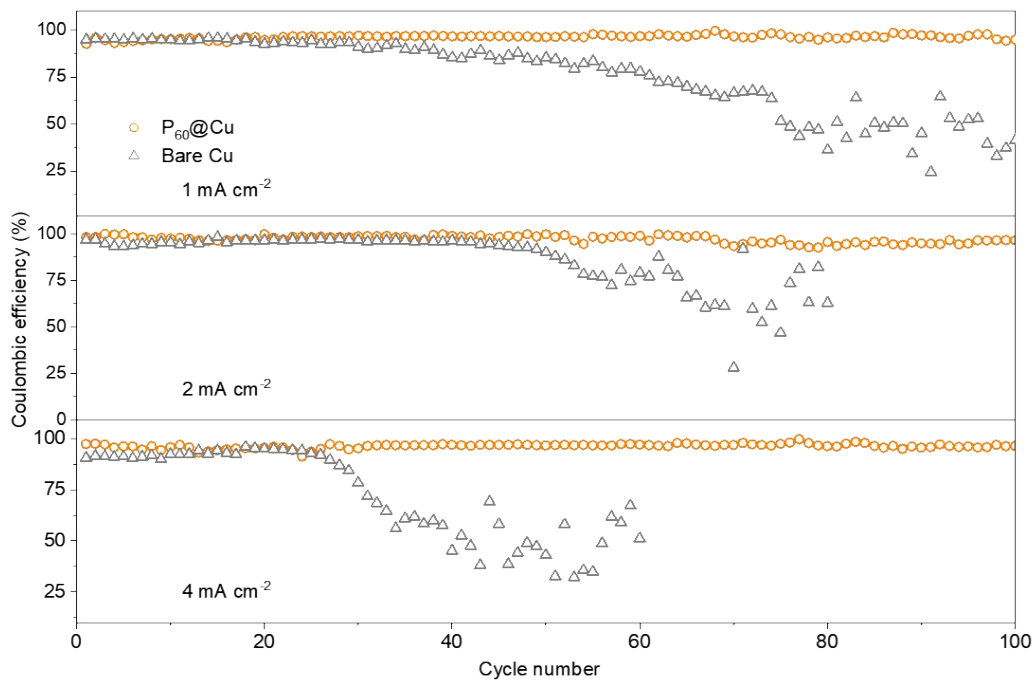
Fig. S28 CEs of different anodes at current densities of 1.0, 2.0, and 4.0 mA cm^{-2}.
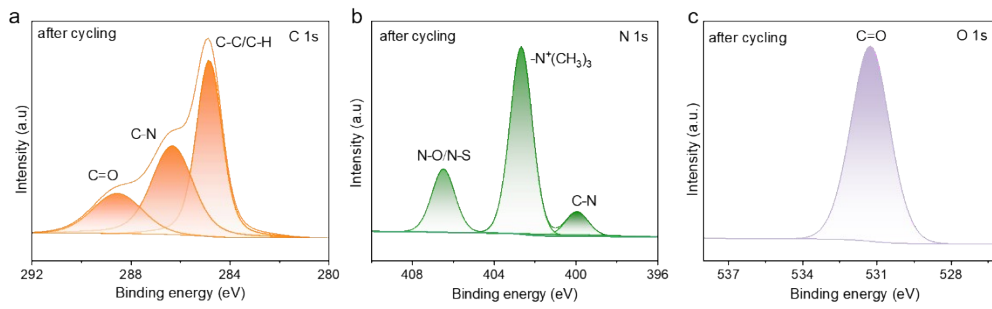
Fig. S29 (a) C 1s, (b) N 1s, and (c) O 1s core-level XPS spectra of PMETAC polymer brushes after 100 cycles.

The typical peaks of PMETAC can be observed after 100 cycles, confirming the stable existence of PMETAC polymer brushes after repeated charge/discharge processes. The peak of N-O/N-S belongs to the residual SEI.
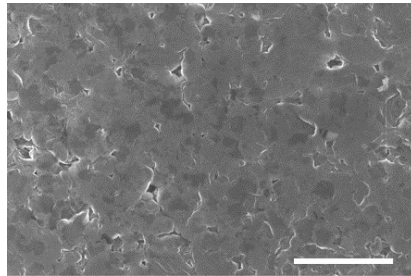
Fig. S30 The morphology of the planar Li layer maintained on the surface of P_{60}@Cu substrate after 100 cycles. The scale bar is 10 μm.
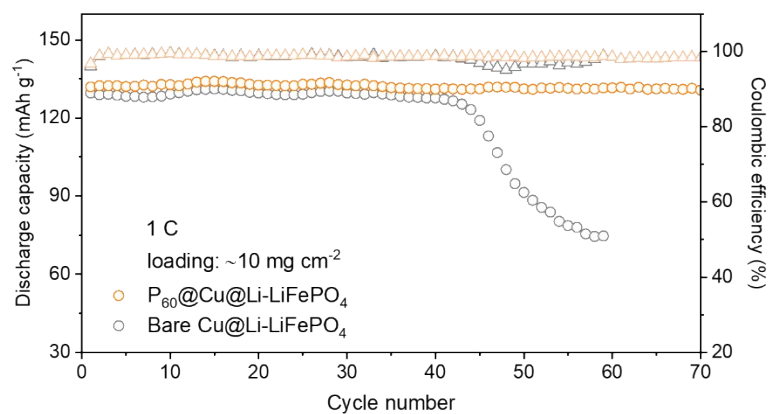
Fig. S31 Cycling performances of P_{60}@Cu@Li-LiFePO$_4$ and Cu@Li-LiFePO$_4$ full cells with a high mass loading of ~10 mg cm^{-2}.
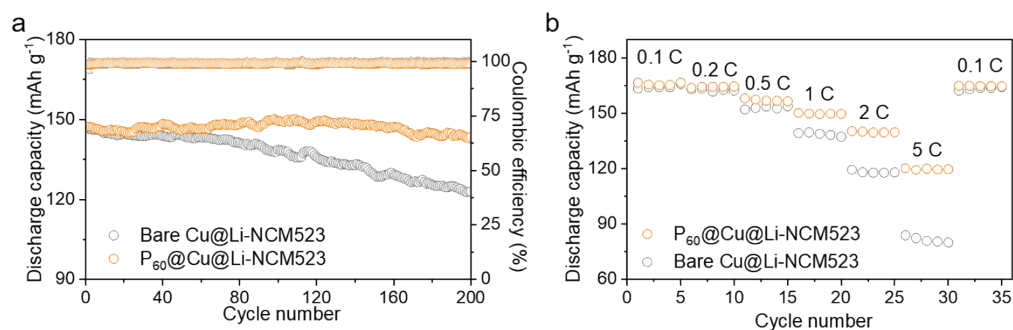
Fig. S32 Electrochemical performances of full cells with NCM523 cathodes. (a) The cycling stabilities of bare Cu@Li-NCM523 and P_{60}@Cu@Li-NCM523 full cells at the current density of 1 C. (b) The rate performances of bare Cu@Li-NCM523 and P_{60}@Cu@Li-NCM523 full cells.
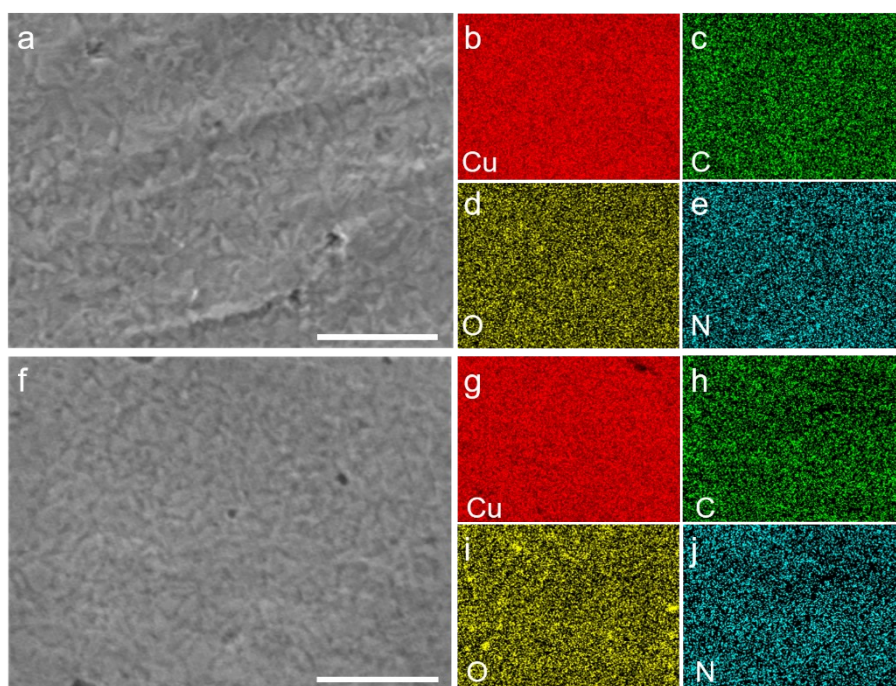
Fig. S33 (a) The initial morphology of PMETAC grafted Cu substrate and (b-e) the corresponding element mappings. (f) The morphology after Li striping and (g-j) the corresponding element mappings. The scale bars are 3 μm.
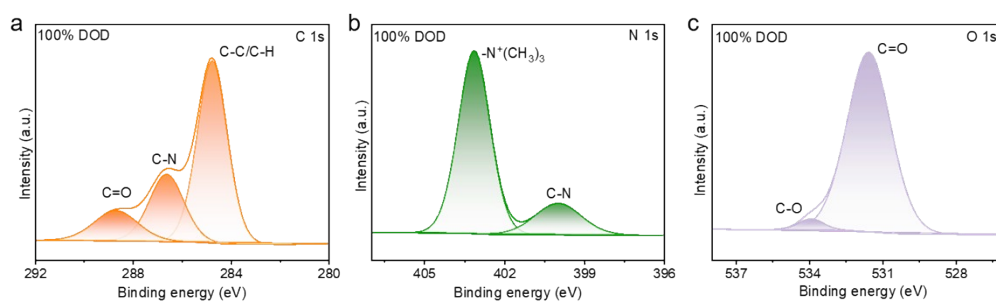
Fig. S34 (a) C 1s, (b) N 1s, and (c) O 1s core-level XPS spectra of PMETAC polymer brushes in P_{60}@Cu@Li-LiFePO$_4$ full cell at 100% DOD state.
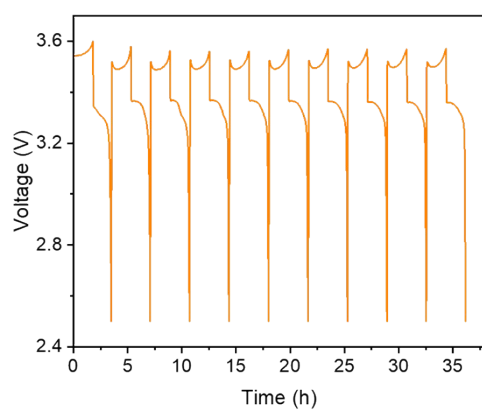
Fig. S35 P_{60}@Cu@Li-LiFePO$_4$ full cell operated under 90% SOC cycling.
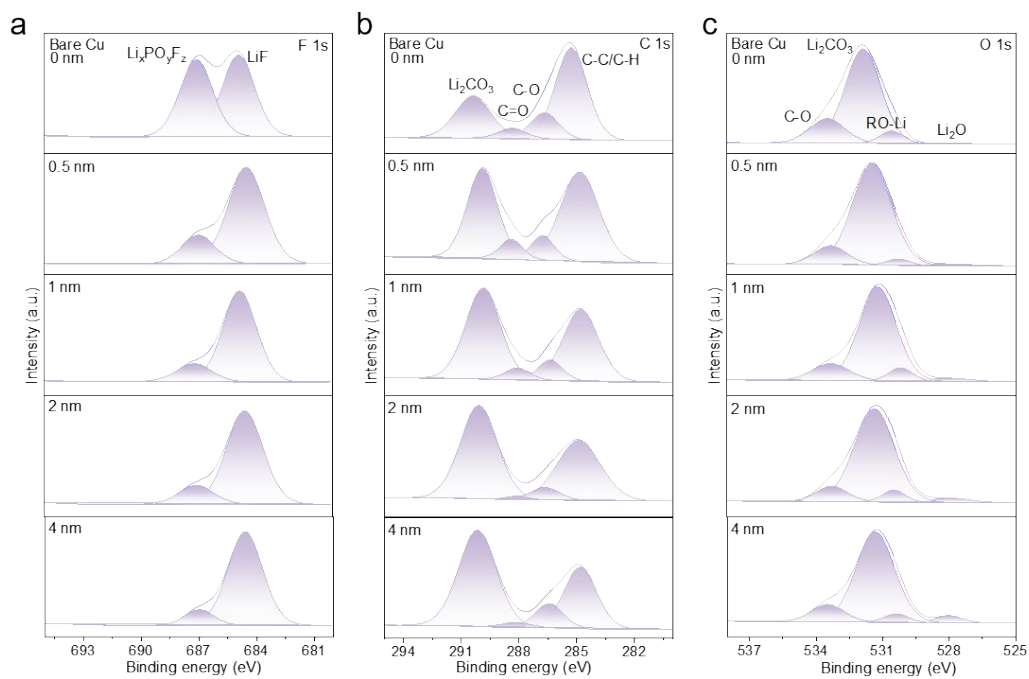
Fig. S36 (a) F 1s, (b) C 1s, and (c) O 1s core-level XPS spectra of SEI on bare Cu foil under 90% SOC cycling.
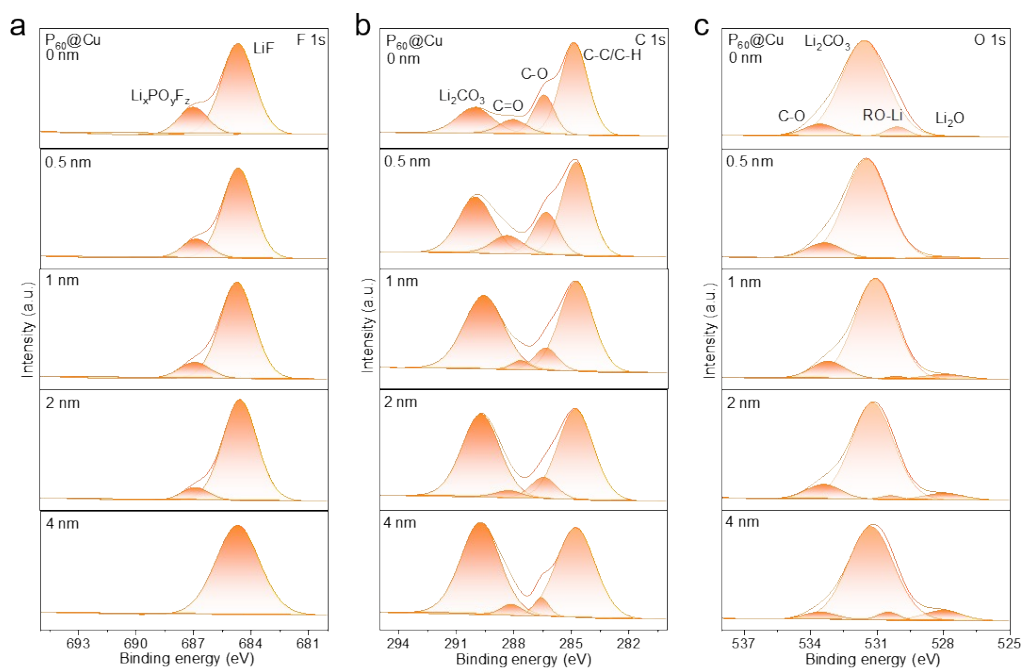
Fig. S37 (a) F 1s, (b) C 1s, and (c) O 1s core-level XPS spectra of SEI on PMETAC grafted Cu substrate under 90% SOC cycling.
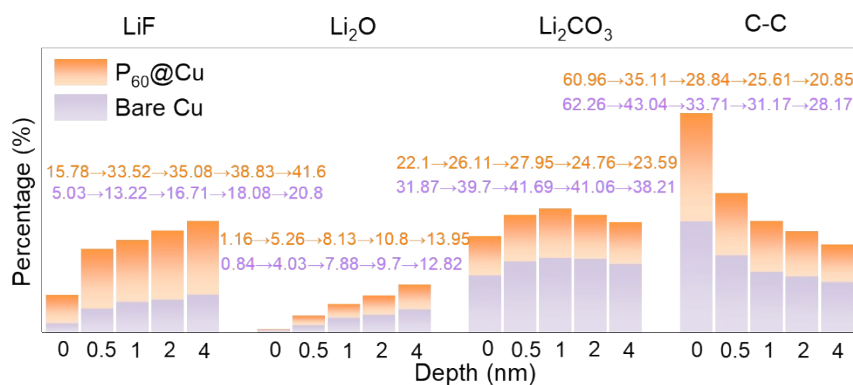
Fig. S38 Comparison of key components of SEI on various substrates under 90% SOC cycling.

It's worth noting that although the specific content values of various components in SEI are slightly different, the XPS results display similar structure and composition distribution and trend to the SEI formed at initial electrodeposition, indicating that the induced inorganic-rich SEI can maintain its structure and composition throughout 90%

SOC cycling.
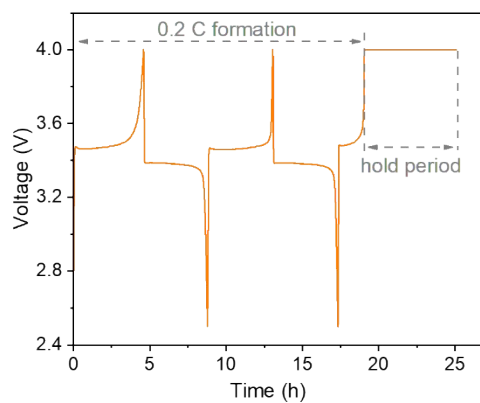
Fig. S39 P_{60}@Cu@Li-LiFePO$_4$ full cell operated under long hold periods at 4V for 6h.
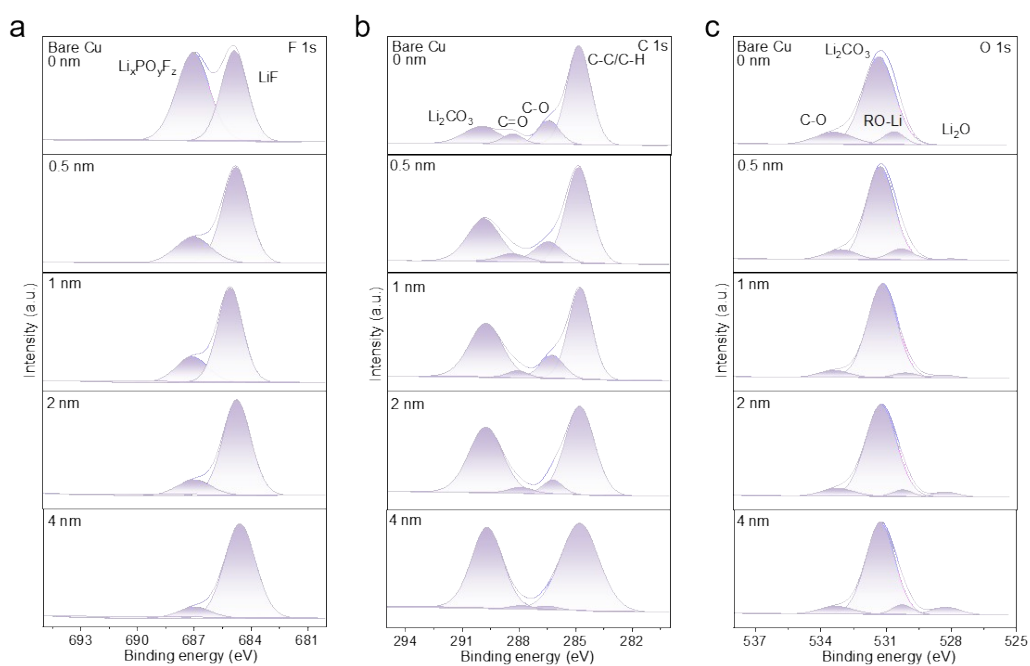
Fig. S40 (a) F 1s, (b) C 1s, and (c) O 1s core-level XPS spectra of SEI on bare Cu foil under 6h hold periods at 4V.
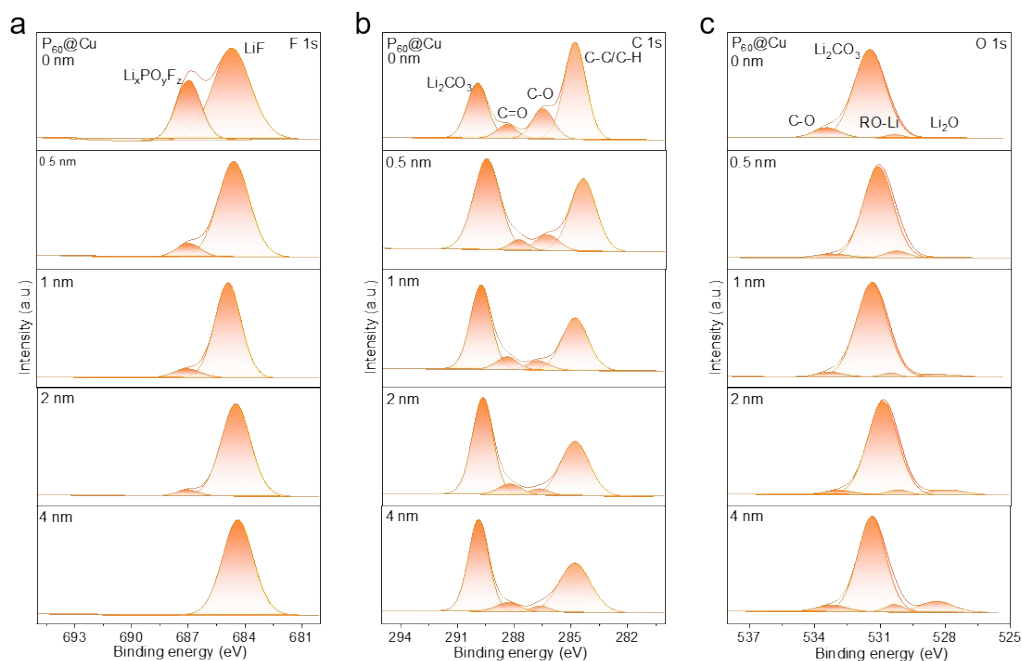
Fig. S41 (a) F 1s, (b) C 1s, and (c) O 1s core-level XPS spectra of SEI on PMETAC grafted Cu substrate under 6h hold periods at 4V.
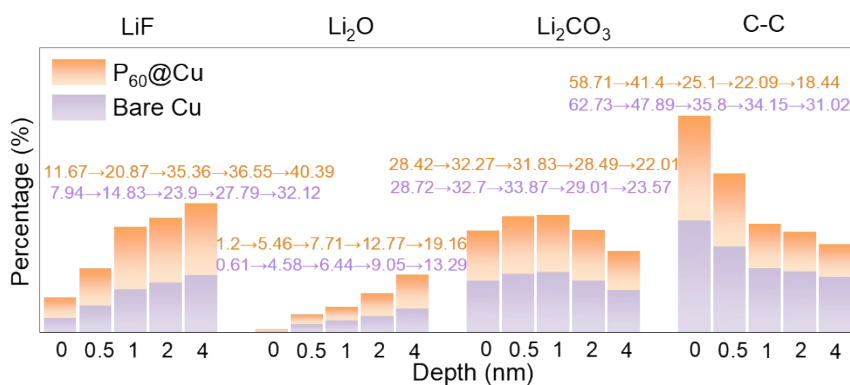
Fig. S42 Comparison of key components of SEI on various substrates under 6h hold periods at 4V.

The similar trend of enhanced inorganic substances and decreased organic substances can be obtained, further revealing that the induced inorganic-rich SEI can maintain its structure and composition throughout long hold periods.
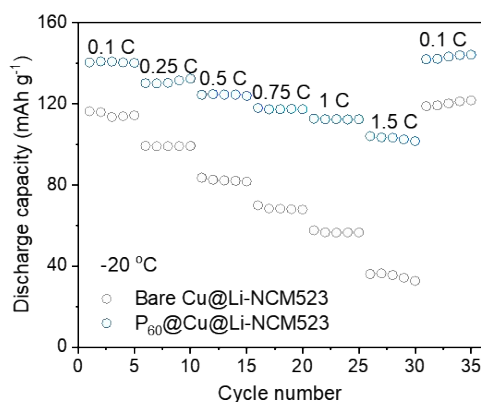
Fig. S43 The rate performances of bare Cu@Li-NCM523 and P$_{60}$@Cu@Li-NCM523 full cells at -20 °C.
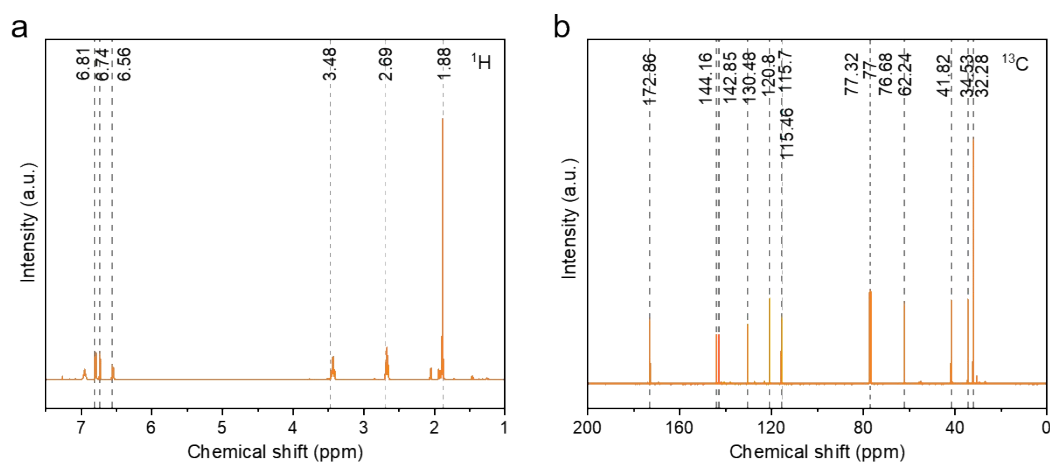
Fig. S44 (a) ^{1}H NMR and (b) ^{13}C NMR of the synthesized initiator 2-bromo-2-methyl-N-[2-(3,4-dihydroxyphenyl)ethyl]propionamide.

Supplementary Table S1. Parameters of the anode-free Li metal pouch cells.

Cell component	cell parameters	
NCM811 cathode	specific capacity	200 mAh g^{-1}
	active material content	96%
	coating weight (each side)	20 mg cm^{-2}

	areal capacity	3.84 mAh cm^{-2}
	electrode sizes	68*60 mm
	Al foil thickness	13 μm
	layers	3 pcs
Cu foil	Cu foil thickness	9 μm
	layers	4 pcs
	electrode sizes	70*62 mm
Electrolyte	E/C ratio	2.6 g Ah^{-1}
Separator	weight	0.62 g
Tab	weight	0.18 g
Packaging foil	weight	1.44 g
Pouch cell	weight	10.74 g
	capacity	0.94 Ah
	specific energy density	324 Wh kg^{-1}

References

1. N. Li, Q. Ye, K. Zhang, H. Yan, C. Shen,B. Wei, K. Xie, *Angew. Chem. Int. Ed.*, 2019, **58**, 18246-18251.

2. J. Langdon, A. Manthiram, *Adv. Funct. Mater.*, 2021, **31**, 2010267.

3. Z. Wang, R. Han, D. Huang, Y. Wei, H. Song, Y. Liu, J. Xue, H. Zhang, F. Zhang, L. Liu, S. Weng, S. Lu, J. Xu, X. Wu, Z. Wei, *ACS Nano*, 2023, **17**, 18103-18113.

4. Y. Xiao, X. Wang, K. Yang, J. Wu, Y. Chao, C. Xi, M. Li, Q. Zhang, Z. Liu, L. Li, Y. Yu, C. Yang, *Energy Storage Mater.*, 2023, **55**, 773-781.

5. L. Zhao, Z. Wu, Z. Wang, Z. Bai, W. Sun, K. Sun, *ACS Nano*, 2022, **16**, 20891-20901.